



Azospirillum brasilense AerC and Tlp4b Cytoplasmic Chemoreceptors Are Promiscuous and Interact with the Two Membrane-Bound Chemotaxis Signaling Clusters Mediating Chemotaxis Responses

Elena E. Ganusova, a Madison Rost, a Anastasia Aksenova, a Mustafa Abdulhussein, a Alisha Holden, a Galadys Alexandre

^aDepartment of Biochemistry and Cellular and Molecular Biology, University of Tennessee, Knoxville, Tennessee, USA

ABSTRACT Chemotaxis in Bacteria and Archaea depends on the presence of hexagonal polar arrays composed of membrane-bound chemoreceptors that interact with rings of baseplate signaling proteins. In the alphaproteobacterium Azospirillum brasilense, chemotaxis is controlled by two chemotaxis signaling systems (Che1 and Che4) that mix at the baseplates of two spatially distinct membrane-bound chemoreceptor arrays. The subcellular localization and organization of transmembrane chemoreceptors in chemotaxis signaling clusters have been well characterized but those of soluble chemoreceptors remain relatively underexplored. By combining mutagenesis, microscopy, and biochemical assays, we show that the cytoplasmic chemoreceptors AerC and Tlp4b function in chemotaxis and localize to and interact with membrane-bound chemoreceptors and chemotaxis signaling proteins from both polar arrays, indicating that soluble chemoreceptors are promiscuous. The interactions of AerC and Tlp4b with polar chemotaxis signaling clusters are not equivalent and suggest distinct functions. Tlp4b, but not AerC, modulates the abundance of chemoreceptors within the signaling clusters through an unknown mechanism. The AerC chemoreceptor, but not Tlp4b, is able to traffic in and out of chemotaxis signaling clusters depending on its level of expression. We also identify a role of the chemoreceptor composition of chemotaxis signaling clusters in regulating their polar subcellular organization. The organization of chemotaxis signaling proteins as large membrane-bound arrays underlies chemotaxis sensitivity. Our findings suggest that the composition of chemoreceptors may fine-tune chemotaxis signaling not only through their chemosensory specificity but also through their role in the organization of polar chemotaxis signaling clusters.

IMPORTANCE Cytoplasmic chemoreceptors represent about 14% of all chemoreceptors encoded in bacterial and archaeal genomes, but little is known about how they interact with and function in large polar assemblies of membrane-bound chemotaxis signaling clusters. Here, we show that two soluble chemoreceptors with a role in chemotaxis are promiscuous and interact with two distinct membrane-bound chemotaxis signaling clusters that control all chemotaxis responses in *Azospirillum brasilense*. We also found that any change in the chemoreceptor composition of chemotaxis signaling clusters alters their polar organization, suggesting a dynamic interplay between the sensory specificity of chemotaxis signaling clusters and their polar membrane organization.

KEYWORDS *Azospirillum*, chemoreceptors, chemotaxis, polar membrane-bound chemoreceptor arrays, chemotaxis signaling clusters

otile bacteria use chemotaxis to navigate toward preferred niches for growth. The best-characterized chemotaxis system is that of *Escherichia coli* (1). It consists of five membrane-bound chemoreceptors (methyl-accepting [MA] chemotaxis proteins [MCPs]) that detect attractants or repellents. Signals detected by MCPs are transmitted across the

Editor Julie A. Maupin-Furlow, University of Florida Department of Microbiology and Cell Science

Copyright © 2023 American Society for Microbiology. All Rights Reserved.

Address correspondence to Gladys Alexandre, galexan2@utk.edu.

The authors declare no conflict of interest.

Received 20 December 2022 Accepted 8 May 2023

membrane through conformational changes to a histidine kinase, CheA, and an adaptor protein, CheW, which interact with a universally conserved cytoplasmic region of MCPs. Chemoreceptor conformational changes induced in response to lower attractant concentrations or higher repellent concentrations stimulate the autophosphorylation activity of CheA from ATP, with the subsequent transfer of the phosphoryl group to the response regulators CheY and CheB. CheY~P has an increased affinity for the flagellar motor switch proteins, with binding triggering a change in the flagellar motor rotational direction to cause a swimming tumble (i.e., reorientation in the swimming direction). CheB~P has increased methylesterase activity on conserved glutamine residues in the cytoplasmic signaling region of membrane-bound chemoreceptors and counteracts their increased methylation caused by the constitutive activity of the CheR methyltransferase. The combined activity of CheR and CheB~P on chemoreceptors adjusts their sensitivity to background conditions.

In E. coli, membrane-bound chemoreceptors form large polar arrays of trimers of chemoreceptor dimers that are coupled with rings of cytoplasmic proteins to form interconnected hexagonal signaling units (2-4). The cytoplasmic tip of trimers of transmembrane chemoreceptor dimers interacts with rings of CheA and CheW that together form the cytoplasmic signaling baseplate (2, 3, 5). A similar hexagonal structure of membranebound arrays has been observed for other bacteria, including Azospirillum brasilense (5-7). Some bacterial species possess multiple chemotaxis systems and chemoreceptors that differ in the numbers of heptad repeats (H) in the 4-helix coiled-coil region of their cytoplasmic signaling domains. Previous work showed that membrane-bound chemoreceptors with different numbers of heptad repeats have different lengths and do not mix in membrane-bound signaling clusters (8). Similarly, some chemotaxis systems comprise only cytoplasmic chemoreceptor arrays that are distinct from the polar membrane-bound chemotaxis arrays. For example, Vibrio cholerae (9) and Rhodobacter sphaeroides (10) possess cytoplasmic chemotaxis arrays in addition to membranebound arrays. Other bacteria such as the alphaproteobacterium A. brasilense possess two spatially distinct membrane-bound arrays, each comprised of chemoreceptors of distinct length classes: 36H and 38H chemoreceptors (7). A. brasilense proteins from two chemotaxis systems, Che1 and Che4, are required and mix at each of the chemotaxis signaling array baseplates (Fig. 1A). Proteins from Che1 and Che4 (CheA1, CheW1, CheA4, and CheW4) interact with each other and with 36H and 38H chemoreceptors and are both required to regulate all chemotaxis responses in this species (11, 12). Mixing Che1 and Che4 chemotaxis signaling proteins at the baseplates of both arrays hints at a molecular mechanism for coordinating chemotaxis signaling originating from two membrane-bound arrays (Fig. 1B). The spatial segregation of membrane-bound chemoreceptors into distinct chemoreceptor arrays can be predicted from sequence analyses based on the numbers of heptad repeats in the signaling regions (13-15). The length class of soluble chemoreceptors can also be derived by determining the number of heptad repeats in the 4-helix coiled-coil regions of the cytoplasmic domains of the chemoreceptors (16), but predicting their subcellular localization relative to other membranebound chemoreceptors encoded in genomes is not as straightforward. About 14% of all chemoreceptors encoded in bacterial and archaeal genomes are predicted to be soluble (13). In contrast to transmembrane chemoreceptors, little is known about how soluble chemoreceptors interact with membrane-anchored polar chemotaxis signaling clusters. Soluble chemoreceptors can form cytoplasmic signaling arrays, as in V. cholerae and R. sphaeroides (17), and others interact with membrane-bound arrays. For example, the soluble TIpD chemoreceptor in Helicobacter pylori forms autonomous chemoreceptor signaling clusters with CheA, CheW, and CheV1 (18). In addition, soluble chemoreceptors may traffic in and out of membrane-bound arrays (13). The A. brasilense genome encodes 11 chemoreceptors predicted to be soluble, including AerC, which is upregulated under nitrogen fixation conditions where it mediates aerotaxis (19). This chemotaxis phenotype and additional evidence suggest that AerC interacts with Che1 and membrane-bound chemoreceptors (19). Che1 and Che4 are required for the assembly and signaling of both the 36H and 38H membrane-bound arrays. These chemoreceptors and chemotaxis

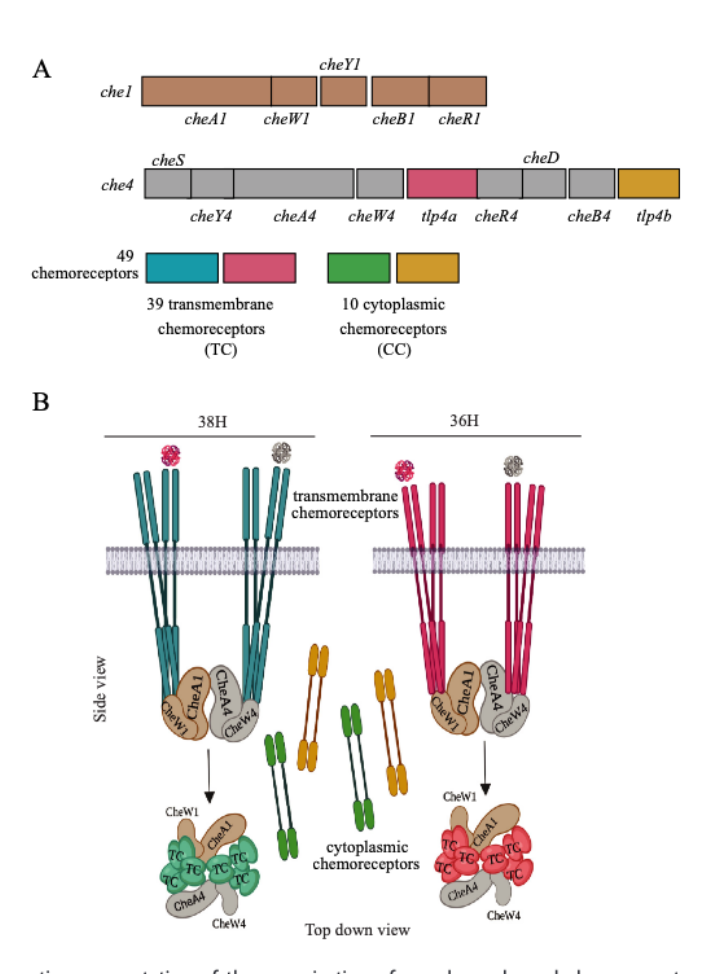


FIG 1 Schematic representation of the organization of membrane-bound chemoreceptor arrays that control chemotaxis in A. brasilense. (A) Genomic organization of genes encoding components of the chemotaxis systems. The chemotaxis genes within each che cluster were either previously characterized or identified by homology searches (see the text for details and references). Most chemoreceptors or transducer-like proteins (Tips) are transmembrane receptors (genes in cerulean and magenta) or cytoplasmic chemoreceptors (genes in green and yellow), and they are encoded elsewhere in the genome. (B) Transmembrane chemoreceptors (in cerulean, magenta, and green) are organized into two spatially distinct chemotaxis signaling arrays, each comprised of membrane-bound chemoreceptors belonging to the 38H heptad repeat length class (in turguoise) or the 36H length class (in dark pink). The histidine kinases CheA1 and CheA4 together with the scaffolding proteins CheW1 and CheW4 form mixed baseplates that are necessary for the structure and signaling functions of both chemoreceptor arrays. Chemoattractant (red stars) or repellent (gray stars) signals perceived by transmembrane chemoreceptors are transduced through the membrane-bound signaling arrays to induce changes in the autophosphorylation activities of CheA1 and CheA4 and subsequent signal transduction events, which are not shown on the scheme. The subcellular localization of cytoplasmic chemoreceptors (in green and yellow) relative to membrane-bound chemotaxis arrays has not been addressed yet, and these are depicted in the scheme separately. Both side-view and topview representations of the chemotaxis arrays are based on published cryo-electron microscopy images (7). (The scheme was created using BioRender [https://biorender.com]).

signaling clusters can be visualized as large polar foci using fusions of fluorescent proteins to representative membrane-bound chemoreceptors. The other chemosensory systems encoded in the *A. brasilense* genome are not involved in chemotaxis, and cryo-electron microscopy (cryo-EM) did not identify any soluble chemoreceptor array (7). Here, we characterize the subcellular localizations and interactions of two soluble chemoreceptors, AerC and Tlp4b, with membrane-bound chemoreceptors and chemotaxis signaling proteins from the 36H and 38H arrays. Our results indicate that AerC and Tlp4b interact with membrane-bound chemoreceptors from both polar arrays and with Che1 and Che4 chemotaxis signaling proteins, although the outcomes of their interactions are not equivalent, hinting at distinct roles. The absence of AerC or Tlp4b as well as any change in the chemoreceptor composition of chemotaxis signaling clusters alter their polar organization, suggesting a dynamic interplay between the sensory specificity of chemotaxis signaling clusters and their polar membrane organization.

RESULTS

Tlp4b, a predicted soluble chemoreceptor encoded in the Che4 system, modulates chemotaxis and wheat root surface colonization. Tlp4b is a predicted soluble chemoreceptor of unknown function encoded in the che4 gene cluster. Tlp4b does not possess any known conserved domains except for the MA (methyl-accepting) domain characteristic of chemotaxis receptors (chemoreceptors here). The encoding of Tlp4b within che4 suggests that it functions during chemotaxis. We constructed an insertion mutation within tlp4b (tlp4b::pKNOCK-Gmr [tlp4b here]) since it is the last gene of the che4 cluster, and we characterized its behavior in gradients of strong chemoeffectors for A. brasilense compared to its parental strain (Sp7 [wild type {WT}]) (Fig. 2). Of the carbon sources tested, the tlp4b mutant was more sensitive than the WT to gradients of malate but was impaired in gradients of butyrate or pyruvate (Fig. 2A). Changes in the swimming behavior of the tlp4b strain were not due to growth defects since the mutant and the WT grew similarly on malate, butyrate, and pyruvate (Table 1). The chemotactic enhancement in gradients of malate or the chemotactic defect in gradients of butyrate or pyruvate of the tlp4b strain could be complemented by the expression of the corresponding parental gene from a broad-host-range plasmid (see Fig. S1 in the supplemental material). These data are consistent with Tlp4b mediating chemotaxis responses. The differential chemotactic responses to spatial gradients of organic acids suggested that the tlp4b strain has altered chemotaxis sensitivity rather than a defect in the direct sensing of these organic acids. To test this hypothesis, we used a spatial gradient for aerotaxis. The aerotaxis response is the strongest in A. brasilense; it takes place within minutes, compared to several days on soft agar plates (20), and aerotaxis tracks with the chemotaxis sensitivity of cells to an air gradient formed in the presence of different carbon sources (21). In this assay, an air gradient is produced by air diffusion into a liquid suspension of cells, to which A. brasilense cells respond by forming an aerotactic band away from the air-liquid interface within \sim 2 min when malate is used as the carbon source (20, 21). The time that it takes for cells to produce a stable aerotactic band is robust and varies with the nature and concentration of the carbon source present as well as the signaling activity of chemoreceptors (21). Compared to the wild type, the tlp4b strain had a short response time for aerotaxis band formation in the presence of malate (Fig. 2B). In the presence of pyruvate, the tlp4b strain had a longer response time than the wild type (Fig. 2B). The aerotaxis band formation response times were similar for the wild-type and tlp4b strains when butyrate at 10 mM was the carbon source, but it was significantly shorter for the tlp4b strain than for the wild type with 20 mM butyrate (Fig. 2C), in support of the tlp4b strain being defective in sensitivity to the gradient. Since chemotaxis is essential for root surface colonization by A. brasilense (22, 23), we also compared wheat root colonization by the $\Delta aerC$ and tlp4b strains and found that the mutant lacking Tlp4b was severely impaired in root surface colonization (Fig. 2D and E), while the mutant lacking AerC was completely null for colonization, at 1 week postinoculation (Fig. 2D and E). The relative abundances of the AerC and Tlp4b proteins in the whole-cell proteomes that we previously analyzed (24) indicated that both Tlp4b and AerC were present at comparable abundances when cells were grown with ammonium chloride and malate (Fig. S2). Therefore, Tlp4b plays a role in the A. brasilense chemotaxis response, and both AerC and Tlp4b contribute to wheat root surface colonization, consistent with their role in chemotaxis.

The localization of AerC-YFP, but not Tlp4b-YFP or other chemotaxis proteins, at fluorescent foci at the cell's poles changes with organic nitrogen availability. Previous studies showed that AerC expression and protein abundance increased when cells were grown under nitrogen fixation conditions (no organic nitrogen and low oxygen concentrations) and that functional AerC-YFP (yellow fluorescent protein) could be detected as polar fluorescent foci in WT cells grown under nitrogen fixation conditions (19). This polar localization was not observed when an organic nitrogen source such as ammonium chloride was present (19). Here, we verified those previous observations (Fig. 3A and C). In contrast to AerC-YFP, Tlp4b-YFP remained as bright foci at the cell poles regardless of the availability of organic nitrogen (Fig. 3B and D). We used the previously characterized Tlp1-YFP (38H) and Tlp4a-YFP (36H) chemoreceptors (7) as well as the soluble chemotaxis signaling kinase CheA1ΔTMX-YFP (CheA1 is produced as two isoforms,

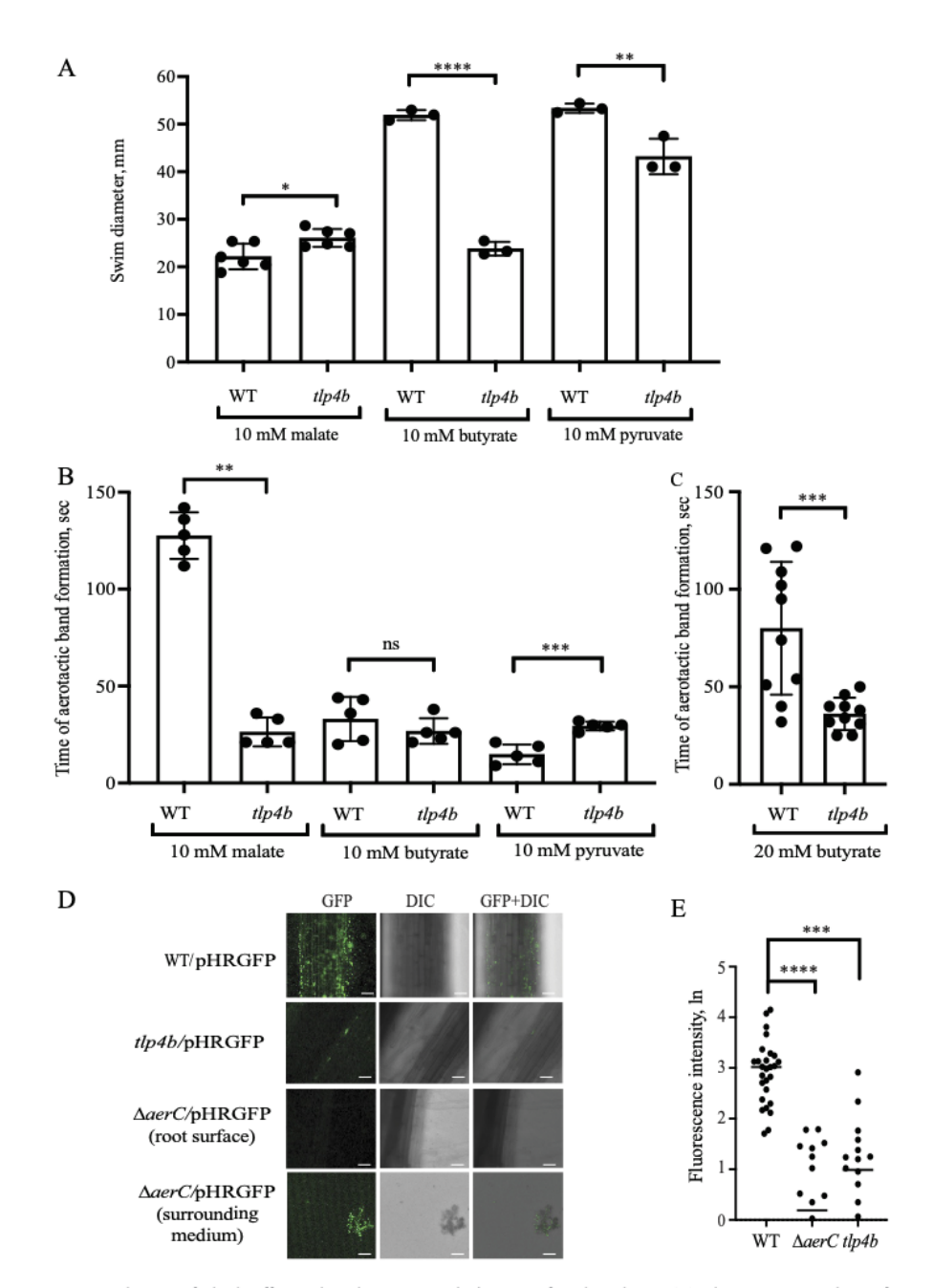


FIG 2 Deletion of tlp4b affects the chemotactic behavior of A. brasilense. (A) Chemotaxis in the soft agar plate assay. (B and C) Response time in the spatial gradient assay for aerotaxis in the presence of 10 mM organic acids (B) or 20 mM butyrate (C). The response time corresponds to the time for the formation of a stable aerotactic band following exposure to the air gradient (in seconds). Asterisks indicate statistically significant differences compared to the value for the wild-type (WT) strain (***, $P \le 0.001$; ****, $P \le 0.0001$; ns, nonsignificant difference [by Student's t test]). (D) Assay of wheat root colonization by the WT, the tlp4b mutant, and the $\Delta aerC$ mutant expressing GFP from the pHRGFP plasmid. Images were taken 96 h after inoculation into semisolid Fahraeus medium. Bars, 20 μ m. DIC, differential interference contrast. (E) Quantification of the fluorescence intensity in the root hair zone normalized to the root autofluorescence. The fluorescence intensity was quantitated using ImageJ Fiji. Asterisks indicate statistically significant differences compared to the value for the wild-type strain (****, $P \le 0.0001$ [by Student's t test]).

with CheA1ΔTMX being the isoform functioning in chemotaxis in *A. brasilense* [25] [called CheA1-YFP here]) or CheA4-YFP (Fig. S4) (7) to probe each of the membrane-bound chemoreceptor arrays. There was no change in the subcellular localization of any of the reporters tested with changes in organic nitrogen availability. The increased polar localization of AerC-YFP in response to a lack of organic nitrogen is thus unique. If the localization of AerC-YFP and Tlp4b-YFP as bright polar foci corresponds to membrane-

Downloaded from https://journals.asm.org/journal/jb on 22 June 2023 by 216.96.204.40

TABLE 1 Growth rates of A. brasilense wild-type and tlp4b mutant strains

	Mean growth rate (h ⁻¹) wi	Mean growth rate (h^{-1}) with 5 mM carbon source \pm SD	
Carbon source	Sp7 (WT)	tlp4b mutant	
Malate ^a	0.61 ± 0.06	0.60 ± 0.04	
Pyruvate ^a	0.29 ± 0.02	0.40 ± 0.01	
Butyrate ^a	1.47 ± 0.05	1.14 ± 0.05	

 $^{^{}o}$ Student's t test (3 biological replicates with 5 technical replicates per biological sample) indicated no significant difference at a P value of <0.05.

bound chemoreceptor arrays, then their polar localization should be abolished in a strain lacking both Che1 (deletion of all *che1* genes [$\Delta che1$]) and Che4 (deletion of all *che4* genes [$\Delta che4$]), as previously shown for other chemoreceptors (7). We observed that the polar localization of AerC-YFP was abolished under conditions of nitrogen fixation in the $\Delta che1$ or the $\Delta che4$ strain as well as the $\Delta che1$ $\Delta che4$ double mutant strain (Fig. 3E). The lack of Che1 or Che4 alone did not produce any detectable change in the polar localization of the Tlp4b-YFP fluorescent foci (Fig. 3F). Tlp4b-YFP fluorescence became mostly nonpolarly localized or diffused only in the absence of both Che1 and Che4 (Fig. 3F). These data are consistent with AerC-YFP and Tlp4-YFP localizing within the two known membrane-bound chemoreceptor arrays and also indicate that AerC-YFP may be able to diffuse in and out of these clusters.

Soluble chemoreceptors interact with membrane-bound chemoreceptors from both arrays, with each other, and with Che1 and Che4 baseplate proteins. Next, we analyzed the subcellular localization of YFP- or cyan fluorescent protein (CFP)-tagged AerC and Tlp4b-YFP relative to Tlp1-YFP, Tlp1-CFP, and Tlp4a-YFP. The fluorescently tagged soluble chemoreceptors AerC and Tlp4b colocalized with each other and with the 38H and 36H membrane-bound chemoreceptors (Fig. 4A). Quantification of the relative subcellular localization of the fluorescent foci indicated that CFP and YFP functions colocalized in roughly 50% of the cells analyzed (Fig. 4B). To confirm the interactions between the AerC and Tlp4b chemoreceptors and components of the chemotaxis signaling arrays, we used a bacterial two-hybrid (BACTH) assay (Fig. S4). We found significant interactions between the soluble chemoreceptors AerC and Tlp4b and membrane-bound chemoreceptors of the 38H (Tlp1) and 36H (Tlp4a) length classes and the chemotaxis signaling proteins CheA1, CheA4, CheW1, and CheW4. We used pulldown assays to verify the physical interactions suggested by microscopy and BACTH assays (Fig. 4A and B). We found that both AerC-GST (glutathione S-transferase) and Tlp4b-GST could interact with Tlp1-YFP and Tlp4a-YFP (Fig. 4C). In a similar assay, we found that CheA1 Δ TMX-GST (CheA1-GST here) and CheA4-GST interacted with AerC-YFP (Fig. 4C) and Tlp4b-YFP (Fig. 4D). We observed that Tlp4b-YFP and, to a lesser extent, AerC-YFP were detected as two bands in Western blots, although we do not know the cause of this observation. The combined data indicate that the AerC and Tlp4b soluble chemoreceptors physically interact with membrane-bound chemoreceptors from both arrays and with chemotaxis signaling proteins that comprise these arrays' baseplates. It follows that AerC and Tlp4b likely populate both the 36H and the 38H membranebound chemoreceptor arrays in A. brasilense.

The absence of soluble AerC or Tlp4b reduces the polar localization of membrane-bound chemoreceptors from both arrays. To evaluate the contribution of soluble chemoreceptors to membrane-bound chemotaxis signaling clusters, we analyzed the subcellular localizations of the 38H chemoreceptor Tlp1-YFP and the 36H chemoreceptor Tlp4b-YFP in strains lacking AerC or Tlp4b. Tlp1-YFP and Tlp4a-YFP localized as bright polar foci in WT cells, as expected (Fig. 5). Tlp1-YFP was diffused or localized as nonpolar foci in the $\Delta aerC$ and tlp4b mutants, with these effects being more pronounced in the tlp4b strain (Fig. 5A and B). Nonpolar Tlp4a-YFP fluorescent foci were more often observed in the $\Delta aerC$ strain than in the WT. This trend was increased in the tlp4b background, with most Tlp4a-YFP being localized as nonpolar foci or diffused throughout the cell. The lack of Tlp4b caused a larger disruption of the polar localization of Tlp1-YFP and Tlp4a-YFP than the lack of AerC. These observations suggest that Tlp4b has a greater contribution to the polar organization of chemotaxis signaling clusters than AerC. We used Western blot assays to probe the

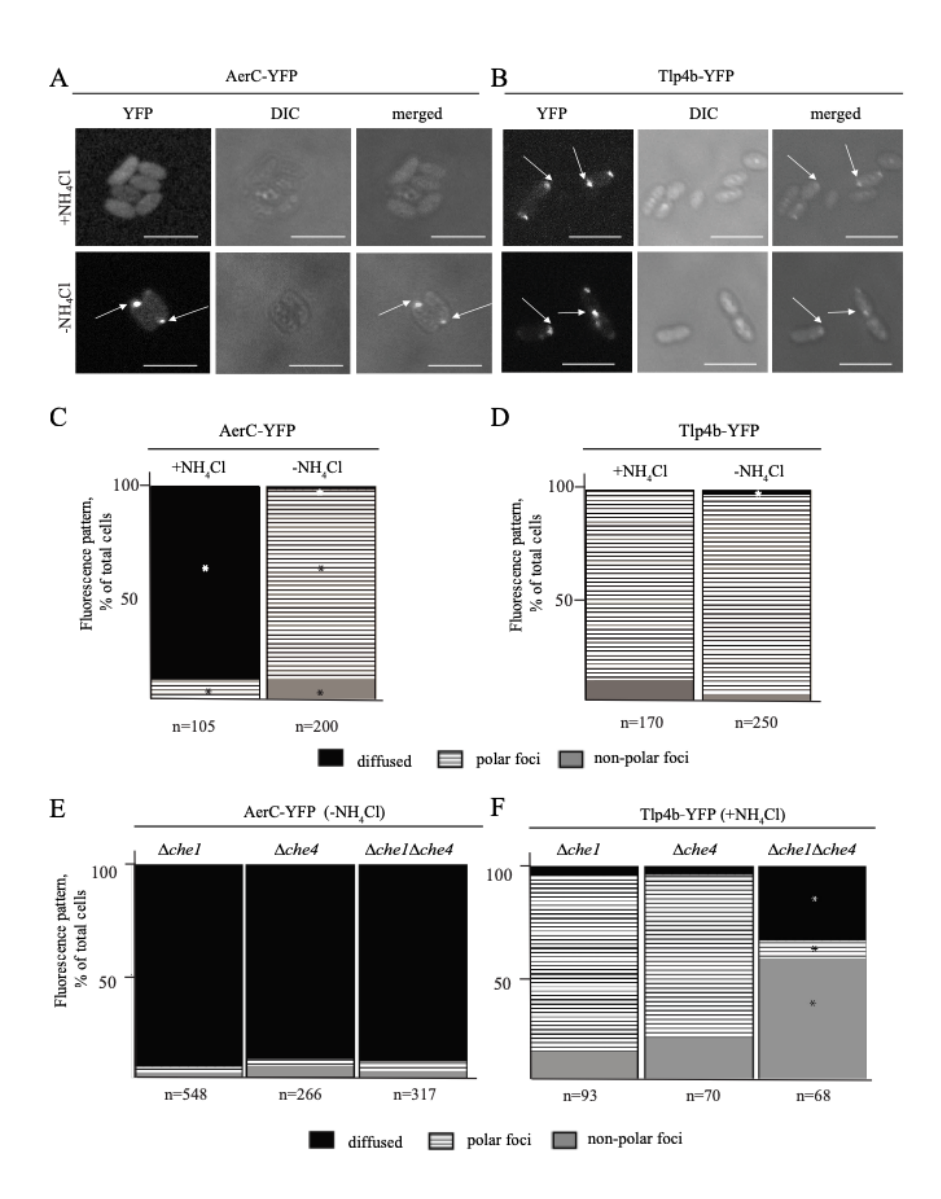


FIG 3 (A and B) The localization of AerC-YFP (A) but not Tlp4b-YFP (B) as fluorescent foci at the cell's poles changes with organic nitrogen availability. Bars, 5 μ m. Arrows indicate fluorescent foci. (C and D) Quantification of the distribution of fluorescent AerC-YFP (C) and Tlp4b-YFP (D) foci in the population of WT cells cultured in MMAB medium with 20 mM ammonium chloride or without ammonium, under conditions of nitrogen fixation. The number of analyzed cells is indicated under each column. The z-score test was used to determine if the fluorescent-focus localization differed significantly in $\Delta aerC$ cells in the presence or absence of ammonium chloride (indicated by *). The localization of the cytoplasmic chemoreceptors AerC-YFP and Tlp4b-YFP is dependent on the presence of the components of the Che1 and Che4 chemotaxis systems. (E and F) Quantification of the distribution of fluorescent AerC-YFP (E) and Tlp4b-YFP (F) in the $\Delta che1$, $\Delta che4$, and $\Delta che1$ $\Delta che4$ mutant strains. The number of analyzed cells is indicated under each column. The z-sore test was used to determine if the fluorescent focus localization differed significantly in the $\Delta che1$ $\Delta che4$ strain compared to the WT (indicated by *).

abundances of Tlp1-YFP and Tlp4a-YFP in the WT, $\Delta aerC$, and tlp4b backgrounds to determine how the observed polar localization effects may occur. We found similar abundances of Tlp1-YFP and Tlp4a-YFP in the WT and $\Delta aerC$ strains but a significantly reduced abundance in the tlp4b strain (Fig. 5D and E). In these experiments, Tlp1-YFP and Tlp4a-YFP are expressed from constitutive promoters on low-copy-number broad-host-range vectors and thus are expected to be similarly expressed in all strain backgrounds. The Western blot results suggest decreased expression or stability of Tlp1-YFP and Tlp4a-YFP in the tlp4b mutant background. Chemotaxis is not abolished in the tlp4b mutant (Fig. 2), indicating that the remaining membrane-bound chemoreceptor clusters are competent for chemotaxis signaling in this mutant. The reduced abundances of Tlp1-YFP and Tlp4a-YFP in the tlp4b strain could be restored

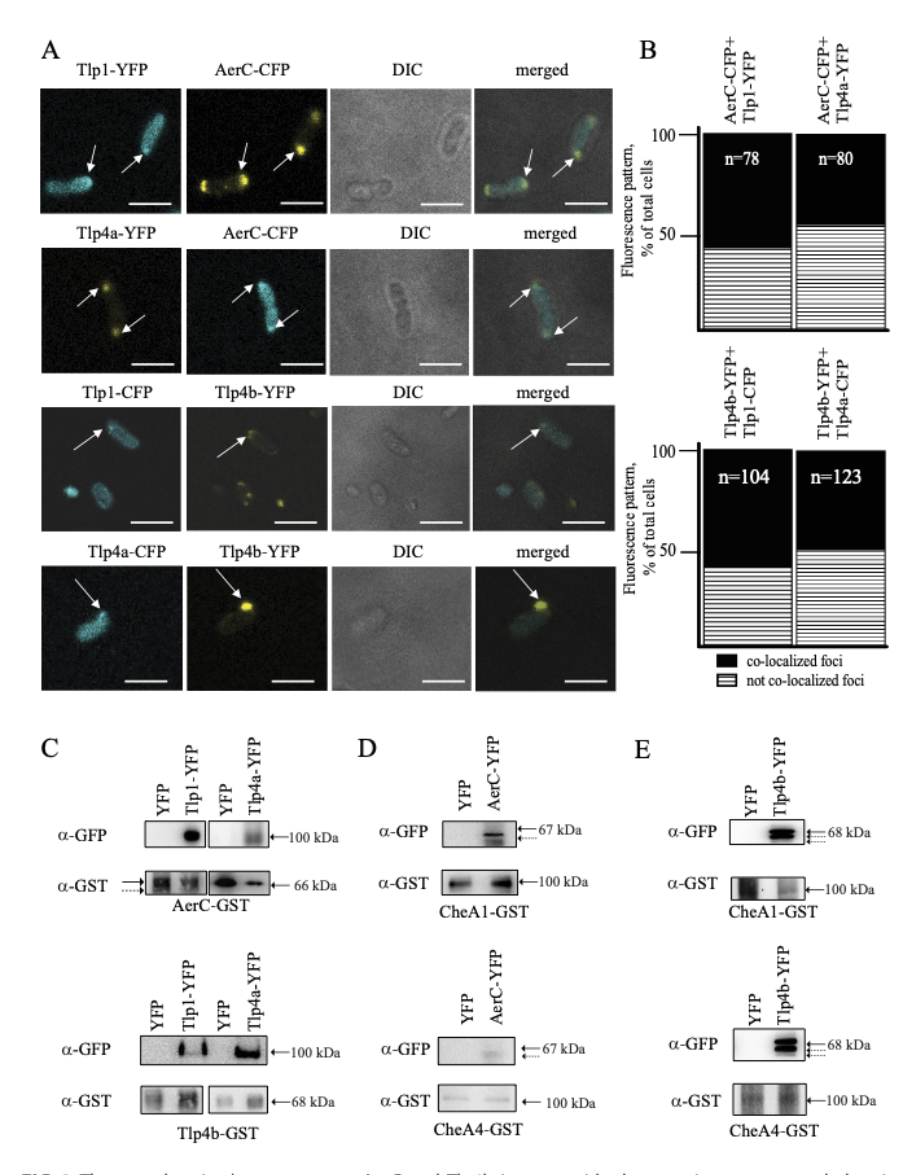


FIG 4 The cytoplasmic chemoreceptors AerC and Tlp4b interact with chemotaxis components belonging to both membrane-bound chemotaxis signaling clusters. (A and B) Colocalization of AerC-CFP with Tlp1-YFP and colocalization of Tlp4a-YFP and Tlp4b-YFP with Tlp1-CFP and Tlp4a-CFP in WT cells. Proteins were expressed from vectors with different origins of replication (pBBR in the case of CFP and pRH in the case of YFP). Arrows indicate the localization of fluorescent foci. Bars, 5 μ m. (C) Interactions of C-terminally GST-tagged AerC or Tlp4b with the transmembrane chemoreceptors Tlp1-YFP and Tlp4a-YFP. The solid arrows indicate ~100-kDa Tlp1-YFP or Tlp4a-YFP or ~66-kDa AerC-GST, while the dashed arrows indicate an unspecific band. (D and E) Interactions of C-terminally GST-tagged CheA1 Δ TMX-YFP and CheA4-YFP with AerC-YFP (C) and Tlp4b-YFP (D). Solid arrows indicate ~100-kDa CheA1 Δ TMX-GST or CheA4-GST, ~67-kDa AerC-YFP, or ~68-kDa Tlp4b-YFP, with the dashed arrow indicating an unspecific band.

by complementation, although some degradation of Tlp4a-YFP was still evident (Fig. S5). These findings together support that Tlp4b, but not AerC, has an additional role in regulating the abundance or stability of chemoreceptors within the signaling clusters, at least under conditions where these chemoreceptors are expressed as fluorescent fusion proteins.

The absence of soluble AerC or Tlp4b disrupts the organization of chemotaxis signaling clusters. The changes in the subcellular localizations of the membrane-bound chemoreceptors Tlp1-YFP and Tlp4a-YFP in the absence of AerC or Tlp4b suggested a disruption of polar chemotaxis signaling clusters. If this hypothesis is correct, we should observe a reduced number and/or size and/or a change in the subcellular localization of polar fluorescent CheA1-YFP and CheA4-YFP foci in both the tlp4b and $\Delta aerC$ backgrounds relative to the WT. In the wild-type background, CheA1-YFP localized as polar or nonpolar foci and was diffused throughout the cell, consistent with previous reports (25) (Fig. 6A and B). Diffused

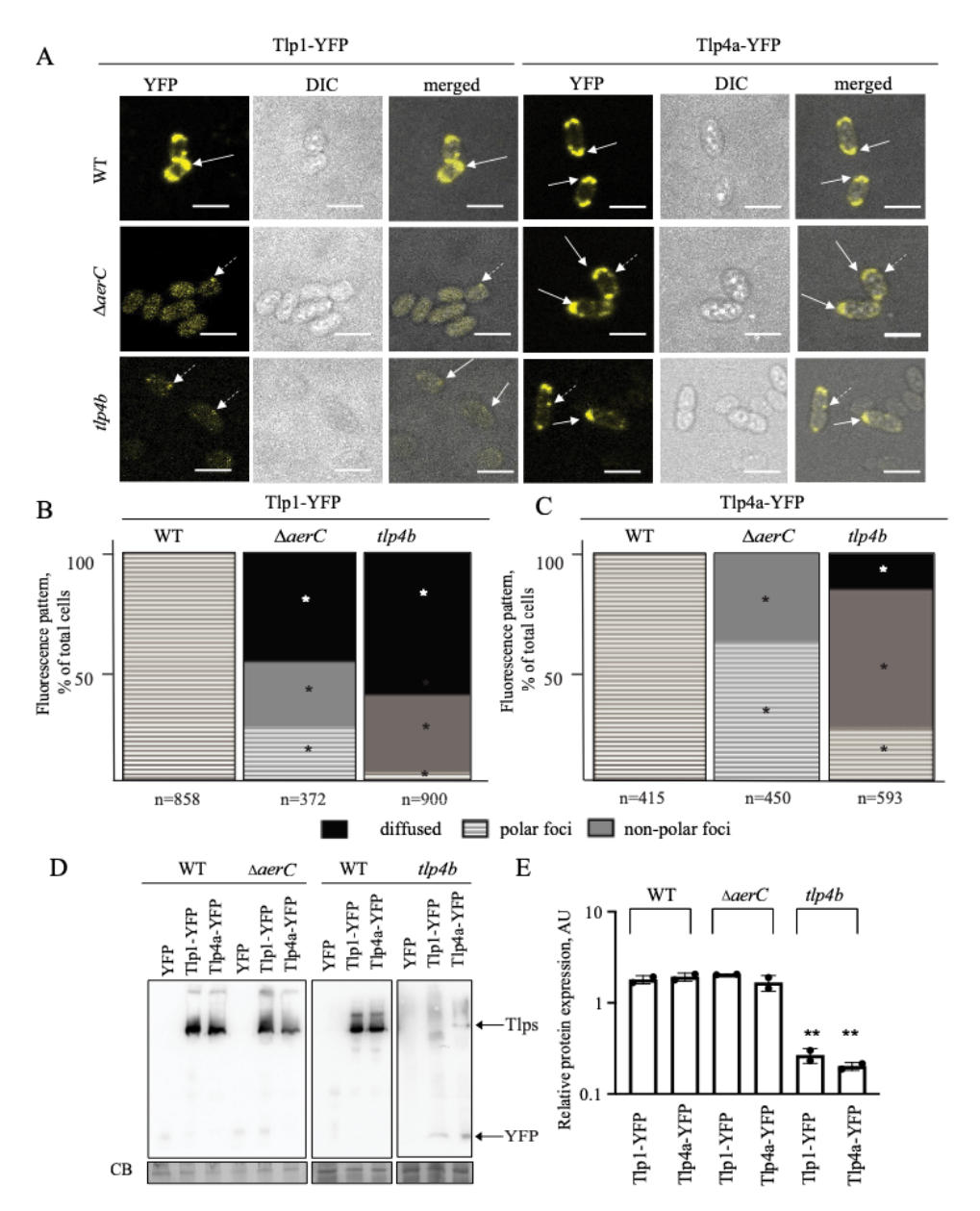


FIG 5 Spatial distribution, expression, and abundance of Tlp1-YFP and Tlp4a-YFP in $\Delta aerC$ and tlp4b mutant cells. (A) Localization of Tlp1-YFP and Tlp4a-YFP in the $\Delta aerC$ and tlp4b mutant backgrounds. Solid arrows point to polar fluorescent foci, while dashed arrows indicate nonpolar foci. Bars, 3 μm. (B and C) Quantification of the distribution of the fluorescent Tlp1-YFP (B) and Tlp4a-YFP (C) foci in the populations of WT, $\Delta aerC$ mutant, and tlp4b mutant cells. The number of analyzed cells is indicated under each column. The z-score test was used to determine if the fluorescent-focus localization in the $\Delta aerC$ and tlp4b strains differed significantly from that of the WT (**, $P \leq 0.01$ [by Student's t test]). (D) Abundances of Tlp1-YFP and Tlp4a-YFP in the WT strain and the $\Delta aerC$ and tlp4b mutant strains determined by Western blot analysis. Coomassie blue staining (CB) of the total proteins was used as a loading control. (E) Densitometric analysis of the Tlp1-YFP and Tlp4a-YFP bands in the WT strain and the $\Delta aerC$ and tlp4b mutants imaged using Image Lab software and analyzed using Image J Fiji. Asterisks indicate statistically significant differences compared to the value for the wild-type strain (***, $P \leq 0.01$ [by Student's t test]). AU, arbitrary units.

CheA1-YFP fluorescence increased and the fraction of cells with polar or nonpolar foci decreased in the $\Delta aerC$ or tlp4b mutant. Polar foci were seldom detected in the tlp4b mutant compared to the $\Delta aerC$ mutant. More cells displayed diffused CheA4-YFP fluorescence and fewer polar foci in the $\Delta aerC$ and tlp4b mutant backgrounds than in the WT background (Fig. 6A and C). Previous work showed that CheY4-YFP, which is encoded in che4, localizes as fluorescent polar foci in a Che1- and Che4-dependent manner, consistent with its interaction with the 38H and 36H chemotaxis signaling clusters (7). CheY4-YFP localized at the poles of WT cells, as expected, but it was mostly diffused or nonpolar in the $\Delta aerC$ or

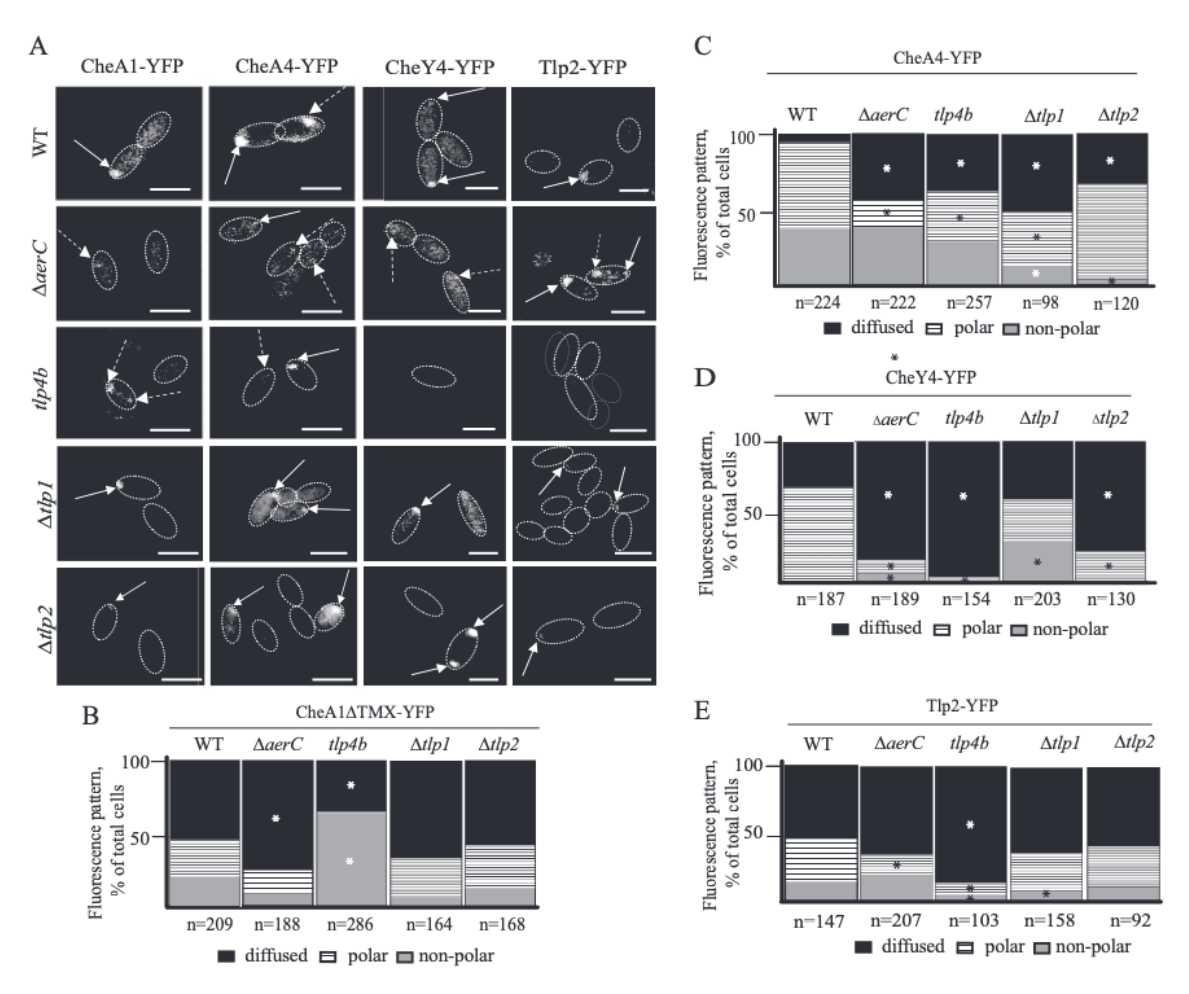


FIG 6 AerC and Tlp4b affect the spatial distribution of the cytoplasmic components of the CheA1 Δ TMX-YFP (CheA1-YFP here) and CheA4-YFP chemotaxis arrays in *A. brasilense* cells. (A) Localization of CheA1-YFP and CheA4-YFP in the Δ aerC and tlp4b mutant backgrounds. The solid arrows point to polar fluorescent foci, while the dashed arrows indicate nonpolar foci. Bars, 3 μ m. (B to E) Quantification of the distribution of the fluorescent CheA1 Δ TMX-YFP (B), CheA4-YFP (C), CheY4-YFP (D), and Tlp2-YFP (E) foci in the populations of WT and Δ aerC, tlp4b, Δ tlp1, and Δ tlp2 mutant cells. The number of analyzed cells is indicated under each column. The z-score test was used to determine if the fluorescent-focus localization in the Δ aerC and tlp4b strains differed significantly from that of the WT. Statistical significance is indicated with *.

tlp4b strain (Fig. 6A, C, and D). The nonpolar Tlp1-YFP and Tlp4a-YFP foci detected in the $\Delta aerC$ and tlp4b backgrounds were found on the sides of the cells and were smaller than the polar foci (Fig. S6). In contrast, both the CheA4-YFP and CheA1-YFP polar and nonpolar foci were relatively small compared to the Tlp1-YFP and Tlp4a-YFP foci (Fig. S6). These results are consistent with the polar organization of chemotaxis signaling clusters depending on the presence of AerC or Tlp4b.

Changes in the composition of chemoreceptors alter the subcellular organization of chemotaxis signaling clusters. Next, we tested the hypothesis that the apparent role of AerC and Tlp4b in maintaining the subcellular organization of chemotaxis signaling clusters is related to their contribution to the composition of chemotaxis signaling cluster chemoreceptors. We used a previously characterized strain lacking the 38H Tlp1 chemoreceptor ($\Delta tlp1$) (22) as well as a mutant lacking Tlp2 ($\Delta tlp2$). The lack of Tlp1 did not produce detectable changes in the distribution of polar fluorescent CheA1-YFP foci (Fig. 6A and B), but it led to increased nonpolar CheY4-YFP fluorescence as well as more pronounced and significant changes in the subcellular localization of CheA4-YFP fluorescent foci (Fig. 6A, C, and D). Similar to Tlp1-YFP or Tlp4a-YFP, Tlp2-YFP produced polar fluorescent foci in the wild-type background and the $\Delta tlp2$ mutant background (Fig. 6A and E). The lack of Tlp1 had a minor effect on the localization of Tlp2-YFP, but the lack of AerC or Tlp4b produced significant changes in the distributions of polar and nonpolar fluorescent foci, with the lack of Tlp4b having the greatest effects (Fig. 6A and E). Therefore, the chemoreceptor

composition of chemotaxis signaling clusters determines their subcellular localization in *A. brasilense*, with the absence of soluble chemoreceptors having consistent disruptive effects.

DISCUSSION

Soluble chemoreceptors are thought to sense intracellular signals (26) to mediate energy taxis (taxis that originates from intracellular energy changes) (14, 20, 27), redox sensing (28–31), or adaptation to the cell metabolic state (32). The cytoplasmic chemoreceptors characterized to date have been found either as autonomous membrane-associated chemotaxis clusters (30) or independent cytoplasmic chemoreceptor arrays (17, 33, 34) or to populate membrane-bound arrays (34-37). Here, we show that at least two soluble chemoreceptors that mediate chemotaxis in A. brasilense are promiscuous and interact with both membrane-bound chemotaxis signaling clusters comprised of Che1 and Che4 proteins and 36H and 38H chemoreceptors. Chemoreceptors are universally assembled into higher-order clusters that consist of 12-nm hexagonal signaling units interconnected by rings of cytoplasmic signaling proteins (3). Cryo-EM imaging indicates that the 36H and 38H membrane chemoreceptor arrays in A. brasilense are assembled as prototypical repeated and interconnected 12-nm hexagonal signaling units (7). Therefore, it is likely that the A. brasilense soluble chemoreceptors populate 36H and 38H membrane-bound chemotaxis signaling arrays as homodimers and contribute to trimers of chemoreceptor dimers within the 12nm hexagonal signaling units.

Our results show that the chemoreceptor composition of chemotaxis signaling clusters affects the polar organization of both the 36H and the 38H membrane-bound chemotaxis signaling clusters. These results are unexpected because the mutants lacking these chemoreceptors are competent for chemotaxis in that they have defective but not null chemotaxis phenotypes. The breaking of large chemoreceptor arrays into smaller ones without abolishing chemotaxis was previously observed in mutants of Treponema denticola lacking a CheW-CheR_{like} protein that populates the chemoreceptor array in this and related species (38). The organization of chemoreceptors as large polar membrane-bound assemblies is responsible for the increased cooperativity and sensitivity during chemotaxis but is not required for chemotaxis (39, 40). The changes in the polar organization of chemotaxis signaling clusters observed in the absence of soluble or membrane-bound chemoreceptors would cause changes in the sensitivity of cells to gradients of various chemoeffectors. Consistent with this hypothesis, the tlp4b mutant displayed altered sensitivity to gradients of organic acids. We do not yet know the exact sensory specificity for Tlp1 or Tlp2, but we note that Tlp1 exhibits defects in aerotaxis as well as chemotaxis to organic acids (22). Some of these defects could be related to changes in chemotaxis sensitivity due to a disruption of the chemotaxis signaling cluster organization reported here. Changes in the presence or absence of chemoreceptors are also expected to alter the sensory specificity and signaling sensitivity of chemotaxis signaling clusters. The findings here suggest that there is a dynamic interplay between the sensory specificity and/or the signaling sensitivity of chemotaxis signaling clusters and their polar organization.

The contribution of AerC to the polar organization of chemotaxis signaling clusters depended on its level of expression. AerC could be either diffused throughout the cells or polarly localized with 36H and 38H membrane-bound chemoreceptors depending on whether the growth conditions supported nitrogen fixation. The other chemoreceptors tested or the chemotaxis proteins did not display such a pattern. The unique contribution of AerC to the polar organization of membrane-bound chemotaxis signaling clusters suggests that it may occupy different discrete positions within the membrane-bound chemoreceptor arrays and/or may interact with other array components with different affinities. One possible unique position would be as homodimers in trimers contacting putative CheW hexameric rings. The existence of hexameric rings of the scaffolding protein CheW was experimentally validated in *E. coli*, where they were proposed to enhance the cooperativity and sensitivity of the chemotaxis signaling array (4). Similar CheW rings in lysed cells of *V. cholerae* were suggested (9), supporting the hypothesis that they may be universally present in chemoreceptor arrays.

We made the puzzling observation that Tlp1-YFP or Tlp4a-YFP was no longer detected by Western blotting in the tlp4b mutant background but not in the $\Delta aerC$ background. This defect was rescued by the expression of parental Tlp4b in the mutant, suggesting a specific role for Tlp4b in modulating the abundance of these chemoreceptors. Similarly, the greatest defects in the polar organization of chemotaxis signaling clusters, as tracked by fluorescent protein fusions to core chemotaxis proteins and chemoreceptors, were observed in the absence of Tlp4b, with this receptor having a consistently greater contribution to this polar organization than AerC or the membrane-bound chemoreceptors tested. We suspect that the role of Tlp4b in modulating chemoreceptor stability contributes to the large impact that a tlp4b mutation has on the polar organization of chemoreceptors. We do not yet know the mechanism(s) underlying the effect of Tlp4b on the abundance of chemoreceptors, and this intriguing function deserves further investigation. One possibility could be related to our recent findings that the lack of CheA1, CheA4, or both affects several nonchemotaxis cellular functions, including nitrogen fixation (24). These results imply that chemotaxis signaling through Che1 and Che4 and, thus, through the 38H and 36H chemotaxis signaling clusters is integrated with the regulation of other cellular functions in this organism. Signaling through Che1 and/or Che4 to these nonchemotaxis functions is likely altered in the tlp4b strain, which would lead to reduced protein expression through an as-yet-unknown posttranslational mechanism and/or the enhanced proteolysis of chemoreceptors. Motility and chemotaxis proteins in Caulobacter crescentus (41) and Sinorhizobium meliloti (37, 42) are degraded by regulated proteolysis in a cell cycle-dependent manner (41, 43). Similar regulation may occur in a Tlp4b-dependent manner in A. brasilense. However, Arapov et al. (42) observed that epitope fusions at the C terminus of the S. meliloti McpU chemoreceptor stabilize the protein by disrupting regulated proteolysis. The YFP C-terminal fusions may stabilize chemoreceptors against proteolysis in A. brasilense. If this is the case, this protection would be specifically lost in a tlp4b mutant. The potential stabilizing effects of C-terminal YFP tags would not account for the patterns of subcellular localization observed in the different strains; for example, Tlp1-YFP and Tlp4a-YFP were detected in the WT and $\Delta aerC$ mutant strains at similar levels by Western blotting, but their patterns of localization in these backgrounds were dissimilar.

The genome of A. brasilense encodes 2 chemotaxis (Che1 and Che4) (12) and 2 chemosensory-like (Che2 and Che3) systems as well as 51 chemoreceptors (Mistdb3.0 [14]). AerC is predicted to be a 38H chemoreceptor, while Tlp4b is predicted to be a 34H chemoreceptor, but it is encoded in the che4 gene cluster together with Tlp4a, a 36H chemoreceptor. Evolutionary considerations have suggested the preferential association of chemoreceptors of a certain length class with specific chemotaxis signaling pathways (44). The genomic organization and the predicted number of heptads in the soluble chemoreceptors analyzed here suggest that AerC would interact with chemoreceptors in the 38H membrane-bound array and that Tlp4b would interact with the chemoreceptors in the 36H membrane-bound array. Instead, our findings imply that 38H and 34H soluble chemoreceptors interact with 36H and 38H membrane-bound chemoreceptor arrays. This apparent discrepancy aligns with findings from an in-depth bioinformatics and phylogenetic analysis of chemoreceptors and chemotaxis pathways in Pseudomonas aeruginosa that suggested that some chemoreceptors can associate with different chemotaxis systems (45). Our data further support some level of promiscuity for soluble chemoreceptors regarding their association with membrane-bound chemotaxis signaling clusters.

MATERIALS AND METHODS

Media, bacterial strains, and growth conditions. The bacterial strains used in this study are listed in Table 2. *A. brasilense* strain Sp7 (ATCC 29145), mutant derivatives, and complemented strains were grown at 28°C in rich tryptone-yeast extract (TY) medium (1 L contains 10 g tryptone and 5 g yeast extract) or Minimal Medium Azospirillum brasilense (MMAB) medium (5 g sodium malate, 3 g K_2HPO_{47} 1 g NAH_2PO_{47} 1 g NH_4CI , 0.3 g $MgSO_4 \cdot 7H_2O$, 0.15 g KCI, 0.01 g $CACI_2 \cdot 2H_2O$, 0.0025 g $CACI_2 \cdot 2H_2O$, and 0.0001 g $CAI_2 \cdot 2H_2O$ mutants were described previously (19, 22) (Table 2). The $CAI_2 \cdot 2H_2O$ mutant was made in this study (see the section on recombinant DNA techniques, below). Biparental mating was performed, as described previously (46), on D plates (8 g Bacto nutrient broth, 0.25 g $CAI_2 \cdot 2H_2O$, 1.0 g $CAI_2 \cdot 2H_2O$, 0.01 g $CAI_2 \cdot 2H_2O$, and 2% $CAI_2 \cdot 2H_2O$, and 2% $CAI_2 \cdot 2H_2O$, 0.01 g $CAI_2 \cdot 2H_2O$,

Downloaded from https://journals.asm.org/journal/jb on 22 June 2023 by 216.96.204.40

TABLE 2 Strains and plasmids used in this study

Strain or plasmid	Description	Source or reference
Strains		
Sp7	Wild type	ATCC 29145
Δa er C	aerC::gusA-Km in Sp7 (Km¹)	19
$\Delta t l p 1$	tlp1::gusA-Km in Sp7 (Km¹)	22
tlp4b	<i>tlp4b</i> ::Gm in Sp7 (Gm ^r)	This study
$\Delta che1$	cheA1::Km in Sp7 (Km¹)	11
∆che4	cheA4::Gm in Sp7 (Gm')	12
Δ che1 Δ che4	cheA1::Km cheA4::Gm in Sp7 (Km ^r Gmr)	12
E. coli Top10	General cloning; F $^-$ mcrA Δ (mrr-hsdRMS-mcrBC) φ 80lacZ Δ M15 Δ lacX74 recA1 araD139 Δ (ara leu) 7697 galU galK rpsL (Str') endA1 nupG	Invitrogen
E. coli BL21(DE3)	$F^- ompT hsdS_B(r_B^- m_B^-) gal dcm$ (DE3)	Invitrogen
E. coli ccdb	F^- mcrA Δ (mrr-hsdRMS-mcrBC) φ 80/acZ Δ M15 Δ lacX74 recA1 ara Δ 139 Δ (ara-leu)7697 galU galK rpsL (Str') endA1 nupG fhuA::IS2	Invitrogen
E. coli BTH101	F ⁻ cya-99 araD139 galE15 galK16 rpsL1 (Str¹) hsdR2 mcrA1 mcrB1	Euromedex
E. coli PIR1	F ⁻ Δlac169 rpoS(Am) robA1 creC510 hsdR514 endA recA1 uidA (ΔMlul)::pir-116	Invitrogen
Plasmids		
pKNOCK-Gm	Suicide vector for gene knockout using insertion mutagenesis; Gm ^r	Addgene
pRK2013	Helper plasmid for triparental mating (ColE1 replicon; Tra Kan)	51
pHRGFP	pBBR-origin plasmid; Tet ^r	47
pDONR221	Gateway-based entry vector; Km ^r	Invitrogen
pCM184	Broad-host-range <i>cre-lox</i> vector for gene deletion	50
pRH004	Gateway-based destination vector expressing proteins fused with CFP at the C terminus; Kmr Cmr	49
pRH005	Gateway-based destination vector expressing proteins fused with YFP at the C terminus; Kmr Cmr	49
pRH-Tlp1(YFP)	pRH005 containing the tlp1 ORF; Kmr Cmr	7
pRH-Tlp1(CFP)	pRH004 containing the tlp1 ORF; Km ^r Cm ^r	7
pRH-Tlp4a(YFP)	pRH005 containing the tĺp4a ORF; Km' Cm'	7
pRH-Tlp4a(CFP)	pRH004 containing the tĺp4a ORF; Km ^r Cm ^r	7
pRH-AerC(YFP)	pRH005 containing the <i>aerC</i> ORF; Km ^r Cm ^r	19
pRH-Tlp2(YFP)	pRH005 containing the <i>tlp2</i> ORF; Km ^r Cm ^r	This study
pRH-AerC(CFP)	pRH004 containing the aerC ORF; Km ^r Cm ^r	19
pRH-Tlp4b(YFP)	pRH005 containing the tlp4b ORF; Km ^r Cm ^r	This study
pRH-CheY4(YFP)	pRH005 containing the <i>cheY4</i> ORF; Km ^r Cm ^r	7
pRH-CheA1ΔTMX(YFP)	pRH005 containing the <i>cheA</i> 1 Δ TMX ORF; Km ^r Cm ^r	25
pRH-CheA4(YFP)	pRH005 containing the <i>cheA4</i> ORF; Km ^r Cm ^r	7
pRK415-Tlp4b	pRK415 containing the <i>tlp4b</i> ORF; Tet ^r	This study
pBBR-Tlp1-CFP	pBBR containing the promoter region and the <i>tlp1</i> ORF; Tet ^r	7
pBBR-Tlp4a-CFP	pBBR containing the promoter region and the <i>tlp4a</i> ORF; Tet'	7
pBBR-AerC-CFP	pBBR containing the promoter region and the aerC ORF; Tet ^r	This study
pDEST24	Gateway-based destination vector expressing proteins fused with GST at the C terminus; Apr	49
pDEST24-CheA1ΔTMX	pDEST24 containing the <i>cheA1ΔTMX</i> ORF; Ap ^r	7
pDEST24-CheA4	pDEST24 containing the <i>cheA4</i> ORF; Apr	7
pDEST24-AerC	pDEST24 containing the <i>aerC</i> ORF; Ap ^r	This study
pDEST24-Tlp4b	pDEST24 containing the <i>tlp4b</i> ORF; Ap'	This study
pKNT25	Derivative of plasmid pSU40 encoding T25 of CyA; Km ^r	55
pKNT25-AerC	pKNT25 containing the aerC ORF; Km ^r	This study
pKNT25-Tlp4b	pKNT25 containing the <i>tlp4b</i> ORF; Km ^r	This study
pUT18C-zip	Derivative of pUT18C in which the leucine zipper of GCN4 is genetically fused in frame to the T18 fragment; Apr	55
pKT25-zip	Derivative of pKT25 in which the leucine zipper of GCN4 is genetically fused in frame to the T25 fragment; Km ^r	55
pUT18	Derivative of plasmid pUC19 encoding T18 of cya; Apr (used for N-terminal fusion)	55
pUT18C	Derivative of plasmid pUC19 encoding T18 of cya; Apr (used for C-terminal fusion)	55
pUT18-CheA1	pUT18 containing <i>cheA1</i> ; Ap ^r	7
pUT18-CheA4	pUT18 containing <i>cheA4</i> ; Ap ^r	7
pUT18-CheW1	pUT18 containing <i>cheW1</i> ; Ap ^r	7
pUT18-CheW4	pUT18 containing <i>cheW4</i> ; Ap ^r	7
pUT18-Tlp1	pUT18 containing <i>tlp1</i> ; Ap ^r	7
pUT18-Tlp4a	pUT18 containing <i>tlp4a</i> ; Ap'	7
pKNT25-Tlp4b	pUTKNT25 containing <i>tlp4b</i> ; Km ^r	This study
pKNT25-AerC	pUTKNT25 containing <i>aerC</i> ; Km ^r	This study

and after conjugation, MMAB medium with the appropriate antibiotics was used for the selection of *A. bra-silense* transconjugants. The following antibiotics were used at the indicated final concentrations unless stated otherwise: ampicillin at 200 μ g/mL, kanamycin at 30 μ g/mL for *A. brasilense* cultures or 50 μ g/mL for *E. coli* cultures, and chloramphenicol at 34 μ g/mL.

Chemotaxis assay. For the swimming assays in petri plates, a single colony from each strain was inoculated into 5 mL of MMAB medium and grown to an optical density at 600 nm (OD₆₀₀) of 0.8. The culture was then washed once with chemotaxis buffer (10 mM potassium phosphate buffer [pH 7.0]), and 5 μ L of the culture was placed on top of MMAB medium solidified with 0.3% (wt/vol) agar (Fisher Scientific) and various carbon sources (malate, pyruvate, succinate, or butyrate) at 10 mM. The plates

were incubated at 28°C for 48 h, and the diameter of the expansion rings was measured. To ensure that differences in the swimming assay were not caused by differences in growth in the presence of various carbon sources, the growth rates of bacteria were calculated based on the growth parameters collected using a microplate absorbance reader with Gen5 software (BioTek Instruments, Winooski, VT, USA).

Spatial gradient assay for aerotaxis. Cells were grown to an OD $_{600}$ of 0.8 in MMAB medium supplemented with malate and ammonium as reported previously (12). Cells were washed three times in chemotaxis buffer and transferred to MMAB medium supplemented with 10 mM malate, butyrate, or pyruvate as the only carbon source. Butyrate was also used at 20 mM. Cells were transferred to an optically flat microcapillary tube (inner dimensions of 0.1 by 2 by 50 mm; Vitro Dynamics, Inc., Rockaway, NJ) by immersing a capillary tube into the suspension of cells. The formation of a stable and tight aerotactic band visualized under a light microscope at a $\times 4$ magnification was video recorded using a Leica mc120 HD camera. The time that it took to form a stable aerotactic band was used to estimate the cells' response sensitivity to the air gradient.

Wheat root colonization assay. Triticum aestivum cv. Jagger (wheat) seeds were used in the root attachment assay. Plant seeds were surface sterilized for 10 min with 90% ethanol and for 20 min with a sterilization buffer containing 1% Triton X-100, 10% bleach, and sterile water. After sterilization, seeds were planted into Fahraeus medium (0.132 g CaCl₂, 0.12 g MgSO₄ · 7H₂O, 0.1 g KH₂PO₄, 0.075 g Na₂HPO₄ · 2H₂O, 0.005 g Fecitrate, and 0.07 mg each of $MnCl_2 \cdot 4H_2O$, $CuSO_4 \cdot 5H_2O$, $ZnCl_2$, H_3BO_3 , and $Na_2MoO_4 \cdot 2H_2O$ [adjusted to pH 7.5] per L) solidified with 4 g/L of agar (semisolid Fahraeus medium) (22). Plates with seeds were placed in the dark for 48 h to germinate. Next, the seedlings were placed into 50-mL Falcon tubes containing 20 mL of semisolid Fahraeus medium and allowed to grow with 8 h of daylight/16 h of darkness at 22°C in the plant growth chamber at 90,000 lx or 1,670 μ mol m⁻² s⁻¹. All assays were performed on germinated and surface-sterilized seedlings that were 5 to 7 days old. For the root attachment assay, the A. brasilense Sp7, $\Delta aerC$, and tlp4b strains harboring the pHRGFP plasmid (47) were cultured in liquid MMAB medium with 10 μ g/mL (final concentration) of tetracycline overnight (28°C at 200 rpm). The cultures were normalized to an OD₆₀₀ of 0.6 using sterile chemotaxis buffer and resuspended in 2 mL of Fahraeus medium in a 15-mL sterile Falcon tube. Twenty microliters of cells was injected into the tubes away from the seedlings. Plants were grown for 96 h after bacterial inoculation. After incubation, the roots were washed three times with sterile chemotaxis buffer, and the roots were subjected to fluorescence microscopy. Images were captured using a Nikon Eclipse 80i fluorescence microscope equipped with a Nikon CoolSnap HQ2 cooled charge-coupled-device camera.

Recombinant DNA techniques. General cloning techniques were used as described previously (48). A. brasilense genomic DNA was isolated using a kit according to the manufacturer's instructions (Promega, Madison, WI). The enzymes for DNA manipulation were purchased from New England BioLabs (NEB) (Ipswich, MA, USA), and the enzymes for PCR amplification were purchased from the TaKaRa Bio Group (USA). To construct a tlp4b insertion mutant, an internal 300-bp region within the tlp4b open reading frame (ORF) and flanked with EcoRI-KpnI was cloned into the pKNOCK-Gm plasmid and inserted into the genome by single homologous recombination to generate a Campbell-type insertion mutation after conjugation. Since the tlp4b gene is the last one in the che4 operon, the tlp4b insertion did not affect the other genes in the che4 operon. The treatment of DNA with restriction enzymes was performed according to the manufacturer's specifications (New England BioLabs, Ipswich, MA). DNA sequencing was performed at the Sanger Sequencing Core Facility (University of Tennessee, Knoxville, TN, USA). Sequence analysis to verify all constructs was performed using BLAST (https://blast.ncbi.nlm.nih.gov/Blast.cgi). The Gateway cloning technique (Invitrogen) was used to generate the Tlp4b protein fused with yellow fluorescent protein at the C terminus in the pRH005 vector (Tlp4b-YFP) or the pDEST24 vector (TIp4b-GST [glutathione S-transferase]) (49). Briefly, the genes of interest were amplified using specific Gateway primers (see Table S1 in the supplemental material) and A. brasilense strain Sp7 genomic DNA. Five microliters of the PCR products was separated on a 0.8% gel for the verification of the insert, and a PCR cleanup kit (Promega) was used to purify the PCR product. The resulting PCR product was used in the BP Clonase (Invitrogen) reaction with the pDONR2.1 vector (Invitrogen). The BP Clonase reaction mixture was then transformed into E. coli Top10 chemically competent cells and plated onto Luria broth (LB) with kanamycin (50 μ g/mL). The colonies obtained after transformation were grown in 5 mL LB with kanamycin (50 $\mu g/mL$), the plasmids were purified using an NEB plasmid purification kit, and the resulting plasmids were used in the LR Clonase reaction (Invitrogen) with the pRH005 or pDEST24 plasmid. The resulting reaction mixtures were transformed into E. coli Top10 competent cells and plated onto LB with kanamycin (50 μ g/mL) in the case of plasmid pRH005 or 50 μ g/mL of ampicillin in the case of plasmid pDEST24. The resulting constructs were introduced into the Sp7 strain using biparental mating as described previously (46). A 606-bp region upstream of the tlp2 open reading frame and spanning to the first 154 bp of the tlp2 coding region was amplified using the primer set for tlp2 (Table S1). The PCR product was cloned into pCR2.1-TOPO (Invitrogen, Carlsbad, CA) for sequence verification. The partial tlp2 region and upstream DNA were digested with Kpnl and Notl and ligated with the pCM184 vector (50) (Table 2) digested with the same enzymes. A 533-bp region downstream of tlp2 was PCR amplified (Table S1) and cloned into pCR2.1 for sequence verification. The tlp2 downstream sequence was excised by digestion with Apal and Sacl and ligated into the pCM184 vector prepared as described above. This construct resulted in the upstream and downstream regions of tlp2 flanking a kanamycin resistance cassette, which replaced a 784-bp coding region of tlp2. The $\Delta tlp2$::Kan^r region was amplified (Table S1) and cloned into pCR2.1-TOPO (Invitrogen) for sequence verification. The construct was excised by EcoRI digestion and ligated into the suicide vector pSUP202 (Table 2). The plasmid was transferred into A. brasilense using triparental mating with pRK2013 (Table 2), and double-homologous recombinant mutants were selected as described previously (51).

Fluorescence microscopy. A. brasilense cells harboring pRH constructs were grown overnight in 5 mL of cells grown in TY medium with chloramphenicol (34 mg/mL). Cells were washed once with chemotaxis buffer and resuspended in MMAB medium. Five microliters of cells was resuspended in MMAB medium and mounted onto a glass slide containing a 100-µL agarose pad (1% low-melting-point agarose in

phosphate-buffered saline [PBS] buffer containing 8 g/L NaCl, 0.2 g/L KCl, 0.24 g/L KH $_2$ PO $_4$ $_7$ and 0.144 g/L Na $_2$ HPO $_4$ [pH 7.0]). The sample was covered with a coverslip. Images were captured using a 63× objective with oil immersion mounted onto a Leica (Wetzlar, Germany) SP8 white light laser confocal system. Images were collected using a 513-nm excitation argon ion laser with an emission maximum of 527 nm in the case of YFP and a 433-nm excitation argon ion laser with an emission maximum of 475 nm in the case of CFP. The total fluorescence of the cells was quantitated using ImageJ Fiji.

We supplemented the medium with 20 mM KNO₃ as the sole nitrogen source to image the Tlp2-YFP fluorescent foci because preliminary experiments indicated that it improved detection. In parallel with confocal microscopy, a Nikon Eclipse 80i fluorescence microscope equipped with a Nikon CoolSnap HQ2 cooled charge-coupled-device camera was used for the quantitation of the cells with polar foci/nonpolar foci/diffused fluorescence. The procedure for cell mounting onto glass slides was similar to that used for confocal microscopy. The quantitation of polar and nonpolar fluorescent foci was done using ImageJ Fiji. Briefly, fluorescent foci or the length of the cells/hypotenuse was measured using the Straight tool. The area under the curve (AUC) representing the brightness of the foci was calculated using the Plot Profile tool. The AUCs determined for the foci of 10 representative cells were plotted on graphs.

Bacterial two-hybrid assay. Protein-protein interactions were analyzed using a bacterial two-hybrid (BACTH) assay, as described previously (52). The genes of interest were fused in frame with one-half of the catalytic domain of the *Bordetella pertussis* adenylate cyclase in either the pKNT25 (low-copy-number) or pUT18C (high-copy-number) vector. A positive protein-protein interaction reconstitutes a functional adenylate cyclase to produce cAMP that activates the *lac* and *mal* operons in *E. coli*, which can be detected quantitatively using a β -galactosidase assay (53). The constructs used in this study are listed in Table 2. Primers used for the construction of plasmids are listed in Table S1. Protein-protein interactions were tested in *E. coli* BTH101 cells cotransformed with the pKNT25 and pUT18 or pUT18C constructs, and transformants were incubated on LB medium with ampicillin (100 μg/mL) and kanamycin (50 μg/mL) for 24 h at 30°C. Several colonies were picked from a plate, inoculated into 5 mL LB with the same antibiotics, and grown at 30°C with shaking (180 rpm) until they reached an OD₆₀₀ of 0.6. Protein-protein interactions were determined using a β -galactosidase assay as described previously (53).

Pulldown assays. A protein pulldown assay was used to confirm the protein-protein interactions detected in the BACTH assay. Gateway cloning and pDEST24 (Invitrogen) were used to generate the AerC-GST and Tlp4b-GST constructs. Other constructs for the pulldown assay are listed in Table 2. Five hundred milliliters of BL21(DE3)(pDEST24 CheA1\DeltaTMX-GST), BL21(DE3)(pDEST24 CheA4-GST), and BL21(DE3)(pDEST24 AerC-GST) was grown to an OD_{600} of 0.5 and induced with 1 mM isopropyl- β -D-thiogalactopyranoside (IPTG; Thermo Scientific) for 3 h. The cells were collected and washed with PBS (pH 8.0). The pellets were resuspended in 1 mL of radioimmunoprecipitation assay (RIPA) buffer (50 mM Tris-HCI, 150 mM NaCI, 1% Triton X-100, 0.1% SDS, 1 mM phenylmethylsulfonyl fluoride, and a protease inhibitor cocktail [1 tablet per 5 mL of buffer] [pH 8.0]) and lysed using a 20-W 110-V sonic Dismembrator (model 120; Fisher Scientific) and the following procedure: 1 min of total sonication at 60% power with a 5-s-on and 10-s-off cycle. The cell debris was removed by centrifugation at 17,000 rpm for 1 h at 4°C. The total protein concentration was quantified using a Bradford assay (54). The lysate (2 mg of total protein) was then applied to equilibrated 2-mL glutathione-agarose resin and incubated for 4 h at 4°C with rotation. Unbound proteins were washed off with 5 bead volumes of PBS. YFP-tagged CheA1ΔTMX-YFP, CheA4-YFP, AerC-YFP, Tlp4b-YFP, Che4a-YFP, Tlp1-YFP, or YFP was expressed in the corresponding mutant backgrounds. Five hundred milliliters of cells was grown overnight to an OD₆₀₀ of 0.8. Protein expression was confirmed using fluorescence microscopy. Cells were collected via centrifugation (3,000 rpm for 15 min at 4°C) and lysed in RIPA buffer using sonication as described above. The protein concentration was quantified using a Bradford assay (Bio-Rad). The whole-cell lysate (2 mg of total protein) was applied to the previously prepared CheA1 Δ TMX-GST/CheA4-GST/AerC-GST/Tlp4b-GST resin and incubated overnight at 4°C with rotation. Unbound proteins were washed off using 10 bead volumes of PBS. Columnbound proteins were eluted with PBS containing 10 mM glutathione.

Western blot analyses. For Western blot analysis, proteins were separated on a 10% SDS-PAGE gel and blotted onto a polyvinylidene difluoride (PVDF) membrane at 90 V for 1 h 10 min. The membrane was blocked with Tris-buffered saline (TBS) with 0.1% Tween 20 and 5% nonfat dry milk. YFP-tagged proteins were detected using an anti-green fluorescent protein (GFP) antibody (7) at a 1:1,000 dilution. CheA1ΔTMX-GST, CheA4-GST, AerC-GST, and Tlp4b-GST column binding was confirmed using anti-GST polyclonal antibody (1:1,000) (Invitrogen). Membranes were incubated with horseradish peroxidase (HRP)-conjugated secondary antibodies (anti-rabbit or anti-mouse; Abcam) at a 1:10,000 dilution and developed using a Bio-Rad imaging system. Western blot analysis to detect protein degradation/abundance was performed as described above, except that 20 mL of cell cultures was used for protein isolation and the sonication cycles were performed for 30 s total with 5 s on and 10 s off. Protein abundance quantitation was performed using ImageJ Fiji.

Statistical analysis. To compare the wild-type and mutant phenotypes such as swimming behaviors, growth rates, Western blot quantitations, and plant root attachment, we used Student's *t* test (GraphPad Prism [version 8] software; GraphPad Software, Inc., San Diego, CA, USA). To analyze cells with various fluorescent foci, we used the z-score test (https://www.socscistatistics.com/tests/ztest/default2.aspx).

SUPPLEMENTAL MATERIAL

Supplemental material is available online only. **SUPPLEMENTAL FILE 1**, PDF file, 1.3 MB.

ACKNOWLEDGMENTS

This research is supported by National Science Foundation grants NSF-MCB 1715185 and NSF-MCB 2130556 (to G.A.). Any opinions, findings, conclusions, or recommendations expressed in this material are those of the authors and do not necessarily reflect the views of the National Science Foundation.

We thank members of the Alexandre laboratory for comments on the manuscript as well as Bonnie Stephens and Matt Russell for construction of the $\Delta tlp2$ mutant and the Tlp2-YFP vector.

REFERENCES

- Parkinson JS, Hazelbauer GL, Falke JJ. 2015. Signaling and sensory adaptation in Escherichia coli chemoreceptors: 2015 update. Trends Microbiol 23:257–266. https://doi.org/10.1016/j.tim.2015.03.003.
- Liu J, Hu B, Morado DR, Jani S, Manson MD, Margolin W. 2012. Molecular architecture of chemoreceptor arrays revealed by cryoelectron tomography of *Escherichia coli* minicells. Proc Natl Acad Sci U S A 109:E1481–E1488. https:// doi.org/10.1073/pnas.1200781109.
- Briegel A, Li X, Bilwes AM, Hughes KT, Jensen GJ, Crane BR. 2012. Bacterial chemoreceptor arrays are hexagonally packed trimers of receptor dimers networked by rings of kinase and coupling proteins. Proc Natl Acad Sci U S A 109:3766–3771. https://doi.org/10.1073/pnas.1115719109.
- Piñas GE, DeSantis MD, Cassidy CK, Parkinson JS. 2022. Hexameric rings of the scaffolding protein CheW enhance response sensitivity and cooperativity in *Escherichia coli* chemoreceptor arrays. Sci Signal 15:eabj1737. https://doi.org/10.1126/scisignal.abj1737.
- Briegel A, Ortega DR, Tocheva EI, Wuichet K, Li Z, Chen S, Müller A, Iancu CV, Murphy GE, Dobro MJ, Zhulin IB, Jensen GJ. 2009. Universal architecture of bacterial chemoreceptor arrays. Proc Natl Acad Sci U S A 106: 17181–17186. https://doi.org/10.1073/pnas.0905181106.
- Parkinson JS, Ames P, Studdert CA. 2005. Collaborative signaling by bacterial chemoreceptors. Curr Opin Microbiol 8:116–121. https://doi.org/10.1016/j.mib.2005.02.008.
- O'Neal L, Gullett JM, Aksenova A, Hubler A, Briegel A, Ortega D, Kjær A, Jensen G, Alexandre G. 2019. Distinct chemotaxis protein paralogs assemble into chemoreceptor signaling arrays to coordinate signaling output. mBio 10:e01757-19. https://doi.org/10.1128/mBio.01757-19.
- Herrera Seitz MK, Frank V, Massazza DA, Vaknin A, Studdert CA. 2014. Bacterial chemoreceptors of different length classes signal independently. Mol Microbiol 93:814–822. https://doi.org/10.1111/mmi.12700.
- Yang W, Alvarado A, Glatter T, Ringgaard S, Briegel A. 2018. Baseplate variability of *Vibrio cholerae* chemoreceptor arrays. Proc Natl Acad Sci U S A 115:13365–13370. https://doi.org/10.1073/pnas.1811931115.
- Porter SL, Wadhams GH, Armitage JP. 2008. Rhodobacter sphaeroides: complexity in chemotactic signalling. Trends Microbiol 16:251–260. https://doi.org/10.1016/j.tim.2008.02.006.
- Bible A, Stephens B, Ortega D, Xie Z, Alexandre G. 2008. Function of a chemotaxis-like signal transduction pathway in modulating motility, cell clumping, and cell length in the alphaproteobacterium *Azospirillum brasilense*. J Bacteriol 190:6365–6375. https://doi.org/10.1128/JB.00734-08.
- Mukherjee T, Kumar D, Burriss N, Xie Z, Alexandre G. 2016. Azospirillum brasilense chemotaxis depends on two signaling pathways regulating distinct motility parameters. J Bacteriol 198:1764–1772. https://doi.org/10.1128/JB.00020-16.
- Collins KD, Lacal J, Ottemann KM. 2014. Internal sense of direction: sensing and signaling from cytoplasmic chemoreceptors. Microbiol Mol Biol Rev 78:672–684. https://doi.org/10.1128/MMBR.00033-14.
- Gumerov VM, Ortega DR, Adebali O, Ulrich LE, Zhulin IB. 2020. MiST 3.0: an updated microbial signal transduction database with an emphasis on chemosensory systems. Nucleic Acids Res 48:D459–D464. https://doi.org/ 10.1093/nar/qkz988.
- Gumerov VM, Andrianova EP, Zhulin IB. 2021. Diversity of bacterial chemosensory systems. Curr Opin Microbiol 61:42–50. https://doi.org/10.1016/j.mib.2021.01.016.
- Alexander RP, Zhulin IB. 2007. Evolutionary genomics reveals conserved structural determinants of signaling and adaptation in microbial chemoreceptors. Proc Natl Acad Sci U S A 104:2885–2890. https://doi.org/10.1073/pnas .0609359104.
- Briegel A, Ortega DR, Mann P, Kjær A, Ringgaard S, Jensen GJ. 2016. Chemotaxis cluster 1 proteins form cytoplasmic arrays in Vibrio cholerae and are stabilized by a double signaling domain receptor DosM. Proc Natl Acad Sci U S A 113:10412–10417. https://doi.org/10.1073/pnas.1604693113.

- Rolig AS, Shanks J, Carter JE, Ottemann KM. 2012. Helicobacter pylori requires TlpD-driven chemotaxis to proliferate in the antrum. Infect Immun 80: 3713–3720. https://doi.org/10.1128/IAI.00407-12.
- Xie Z, Ulrich LE, Zhulin IB, Alexandre G. 2010. PAS domain containing chemoreceptor couples dynamic changes in metabolism with chemotaxis. Proc Natl Acad Sci U S A 107:2235–2240. https://doi.org/10.1073/pnas.0910055107.
- Alexandre G, Greer SE, Zhulin IB. 2000. Energy taxis is the dominant behavior in Azospirillum brasilense. J Bacteriol 182:6042–6048. https://doi .org/10.1128/JB.182.21.6042-6048.2000.
- O'Neal L, Ryu M-H, Gomelsky M, Alexandre G. 2017. Optogenetic manipulation of cyclic di-GMP (c-di-GMP) levels reveals the role of c-di-GMP in regulating aerotaxis receptor activity in *Azospirillum brasilense*. J Bacteriol 199:e00020-17. https://doi.org/10.1128/JB.00020-17.
- Greer-Phillips SE, Stephens BB, Alexandre G. 2004. An energy taxis transducer promotes root colonization by *Azospirillum brasilense*. J Bacteriol 186:6595–6604. https://doi.org/10.1128/JB.186.19.6595-6604.2004.
- O'Neal L, Akhter S, Alexandre G. 2019. A PilZ-containing chemotaxis receptor mediates oxygen and wheat root sensing in *Azospirillum brasilense*. Front Microbiol 10:312. https://doi.org/10.3389/fmicb.2019.00312.
- 24. Ganusova EE, Vo LT, Abraham PE, O'Neal Yoder L, Hettich RL, Alexandre G. 2021. The *Azospirillum brasilense* core chemotaxis proteins CheA1 and CheA4 link chemotaxis signaling with nitrogen metabolism. mSystems 6: e01354-20. https://doi.org/10.1128/mSystems.01354-20.
- Gullett JM, Bible A, Alexandre G. 2017. Distinct domains of CheA confer unique functions in chemotaxis and cell length in *Azospirillum brasilense* Sp7. J Bacteriol 199:e00189-17. https://doi.org/10.1128/JB.00189-17.
- Lacal J, García-Fontana C, Muñoz-Martínez F, Ramos JL, Krell T. 2010. Sensing
 of environmental signals: classification of chemoreceptors according to the
 size of their ligand binding regions. Environ Microbiol 12:2873–2884. https://
 doi.org/10.1111/j.1462-2920.2010.02325.x.
- Schweinitzer T, Mizote T, Ishikawa N, Dudnik A, Inatsu S, Schreiber S, Suerbaum S, Aizawa S-I, Josenhans C. 2008. Functional characterization and mutagenesis of the proposed behavioral sensor TlpD of *Helicobacter* pylori. J Bacteriol 190:3244–3255. https://doi.org/10.1128/JB.01940-07.
- Hong CS, Shitashiro M, Kuroda A, Ikeda T, Takiguchi N, Ohtake H, Kato J. 2004. Chemotaxis proteins and transducers for aerotaxis in Pseudomonas aeruginosa. FEMS Microbiol Lett 231:247–252. https://doi.org/10.1016/ S0378-1097(04)00009-6.
- Reuter M, van Vliet AH. 2013. Signal balancing by the CetABC and CetZ chemoreceptors controls energy taxis in *Campylobacter jejuni*. PLoS One 8:e54390. https://doi.org/10.1371/journal.pone.0054390.
- Collins KD, Andermann TM, Draper J, Sanders L, Williams SM, Araghi C, Ottemann KM. 2016. The Helicobacter pylori CZB cytoplasmic chemoreceptor TlpD forms an autonomous polar chemotaxis signaling complex that mediates a tactic response to oxidative stress. J Bacteriol 198:1563–1575. https:// doi.org/10.1128/JB.00071-16.
- Perkins A, Tudorica DA, Amieva MR, Remington SJ, Guillemin K. 2019. Helicobacter pylori senses bleach (HOCl) as a chemoattractant using a cytosolic chemoreceptor. PLoS Biol 17:e3000395. https://doi.org/10.1371/ journal.pbio.3000395.
- de Beyer JA, Szöllössi A, Byles E, Fischer R, Armitage JP. 2019. Mechanism of signalling and adaptation through the Rhodobacter sphaeroides cytoplasmic chemoreceptor cluster. Int J Mol Sci 20:5095. https://doi.org/10 .3390/iims20205095.
- Briegel A, Wong ML, Hodges HL, Oikonomou CM, Piasta KN, Harris MJ, Fowler DJ, Thompson LK, Falke JJ, Kiessling LL, Jensen GJ. 2014. New insights into bacterial chemoreceptor array structure and assembly from electron cryotomography. Biochemistry 53:1575–1585. https://doi.org/10.1021/bi5000614.
- Jones CW, Armitage JP. 2017. Essential role of the cytoplasmic chemoreceptor TlpT in the de novo formation of chemosensory complexes in

- Rhodobacter sphaeroides. J Bacteriol 199:e00366-17. https://doi.org/10.1128/JB.00366-17.
- Meier VM, Scharf BE. 2009. Cellular localization of predicted transmembrane and soluble chemoreceptors in Sinorhizobium meliloti. J Bacteriol 191:5724–5733. https://doi.org/10.1128/JB.01286-08.
- Hou S, Larsen RW, Boudko D, Riley CW, Karatan E, Zimmer M, Ordal GW, Alam M. 2000. Myoglobin-like aerotaxis transducers in Archaea and Bacteria. Nature 403:540–544. https://doi.org/10.1038/35000570.
- Meier VM, Muschler P, Scharf BE. 2007. Functional analysis of nine putative chemoreceptor proteins in *Sinorhizobium meliloti*. J Bacteriol 189:1816–1826. https://doi.org/10.1128/JB.00883-06.
- Muok AR, Ortega DR, Kurniyati K, Yang W, Maschmann ZA, Sidi Mabrouk A, Li C, Crane BR, Briegel A. 2020. Atypical chemoreceptor arrays accommodate high membrane curvature. Nat Commun 11:5763. https://doi.org/10.1038/s41467-020-19628-6.
- 39. Bray D. 2002. Bacterial chemotaxis and the question of gain. Proc Natl Acad Sci U S A 99:7–9. https://doi.org/10.1073/pnas.022641699.
- Sourjik V, Berg HC. 2004. Functional interactions between receptors in bacterial chemotaxis. Nature 428:437–441. https://doi.org/10.1038/nature02406.
- Grünenfelder B, Tawfilis S, Gehrig S, ØSterås M, Eglin D, Jenal U. 2004. Identification of the protease and the turnover signal responsible for cell cycle-dependent degradation of the Caulobacter FliF motor protein. J Bacteriol 186: 4960–4971. https://doi.org/10.1128/JB.186.15.4960-4971.2004.
- Arapov TD, Saldaña RC, Sebastian AL, Ray WK, Helm RF, Scharf BE. 2020. Cellular stoichiometry of chemotaxis proteins in *Sinorhizobium meliloti*. J Bacteriol 202:e00141-20. https://doi.org/10.1128/JB.00141-20.
- Tsai JW, Alley MR. 2001. Proteolysis of the Caulobacter McpA chemoreceptor is cell cycle regulated by a ClpX-dependent pathway. J Bacteriol 183:5001–5007. https://doi.org/10.1128/JB.183.17.5001-5007.2001.
- Wuichet K, Zhulin IB. 2010. Origins and diversification of a complex signal transduction system in prokaryotes. Sci Signal 3:ra50. https://doi.org/10 .1126/scisignal.2000724.
- Ortega DR, Fleetwood AD, Krell T, Harwood CS, Jensen GJ, Zhulin IB. 2017.
 Assigning chemoreceptors to chemosensory pathways in *Pseudomonas*

- aeruginosa. Proc Natl Acad Sci U S A 114:12809–12814. https://doi.org/10.1073/pnas.1708842114.
- Hauwaerts D, Alexandre G, Das SK, Vanderleyden J, Zhulin IB. 2002. A major chemotaxis gene cluster in Azospirillum brasilense and relationships between chemotaxis operons in alpha-proteobacteria. FEMS Microbiol Lett 208:61–67. https://doi.org/10.1111/j.1574-6968.2002.tb11061.x.
- Ramos HJO, Roncato-Maccari LDB, Souza EM, Soares-Ramos JRL, Hungria M, Pedrosa FO. 2002. Monitoring Azospirillum-wheat interactions using the gfp and gusA genes constitutively expressed from a new broad-host range vector. J Biotechnol 97:243–252. https://doi.org/10.1016/s0168-1656(02)00108-6.
- Sambrook J, Russell DW. 2001. Molecular cloning: a laboratory manual, 3rd ed. Cold Spring Harbor Laboratory Press, Cold Spring Harbor, NY.
- Hallez R, Letesson JJ, Vandenhaute J, De Bolle X. 2007. Gateway-based destination vectors for functional analyses of bacterial ORFeomes: application to the Min system in *Brucella abortus*. Appl Environ Microbiol 73: 1375–1379. https://doi.org/10.1128/AEM.01873-06.
- Marx CJ, Lidstrom ME. 2002. Broad-host-range cre-lox system for antibiotic marker recycling in gram-negative bacteria. Biotechniques 33:1062–1067. https://doi.org/10.2144/02335rr01.
- Figurski DH, Helinski DR. 1979. Replication of an origin-containing derivative of plasmid RK2 dependent on a plasmid function provided in trans. Proc Natl Acad Sci U S A 76:1648–1652. https://doi.org/10.1073/pnas.76.4.1648.
- Ouellette SP, Gauliard E, Antosová Z, Ladant D. 2014. A Gateway-compatible bacterial adenylate cyclase-based two-hybrid system. Environ Microbiol Rep 6:259–267. https://doi.org/10.1111/1758-2229.12123.
- Ramsay JP, Williamson NR, Spring DR, Salmond GP. 2011. A quorum-sensing molecule acts as a morphogen controlling gas vesicle organelle biogenesis and adaptive flotation in an enterobacterium. Proc Natl Acad Sci U S A 108:14932–14937. https://doi.org/10.1073/pnas.1109169108.
- Bradford MM. 1976. A rapid and sensitive method for the quantitation of microgram quantities of protein utilizing the principle of protein-dye binding. Anal Biochem 72:248–254. https://doi.org/10.1016/0003-2697(76)90527-3.
- Rowland MA, Deeds EJ. 2014. Crosstalk and the evolution of specificity in two-component signaling. Proc Natl Acad Sci U S A 111:5550–5555. https:// doi.org/10.1073/pnas.1317178111.